Direct Power Flow Controller—A New Concept in Power Transmission

Youjun Zhang, Guoqing Lu, Wajid Ali Khan, Yuzhen Zhang, and Qixin Zhu

***Abstract*—For power transmission in grid, a new concept of direct power flow controller (DPFC) was proposed based on single-stage ac–ac converter with controllable phase and amplitude. By connecting its regulated output compensation voltage with grid in series, DPFC is able to regulate the amplitude and phase angle of grid node voltage, and thus can effectively control active and reactive power flow in grid, respectively and simultaneously. Compared with unified power flow controller (UPFC), DPFC also has a parallel transformer and a series transformer but has no dc energy storage element that easily leads to high equipment failure rate. Furthermore, UPFC is similar to two-stage conversion circuit, while DPFC has only one-stage conversion circuit, which consists of three single-phase buck-type ac units and a three-phase output filter. With respect to the input voltage of DPFC basic circuit, the phase regulation range of its output compensation voltage is 60°, which is easy to extend to 360° with two selection switches changing the connection groups of the input and output transformer. The topology structure and operational principle of DPFC were presented, and the experimental results of a prototype showed its feasibility and verified the theoretical analysis of DPFC.**

***Index Terms*—AC–AC converter with controllable phase and amplitude (ACCPA), compensation voltage, direct power flow controller (DPFC), grid voltage, phase regulation, power transmission.**

I. Introduction

FLEXIBLE ac transmission system (FACTS) technology has been widely applied in power grid, such as improving the power transmission ability and the stability of power system and increasing the effectiveness of power flow control [1]–[4].

Usually shunt FACTS devices are employed to compensate the reactive power in grid and prevent grid voltage from dropping [5], [6], which are in essence var loads or var sources and cannot control the current in individual branches and the active power flow in meshed systems effectively. Static synchronous compensator (STATCOM) [7]–[11] and static var compensator [12]–[15] are two kinds of widely used shunt FACTS devices.

Gate turn-OFF thyristor-controlled series capacitor [16], thyristor-controlled series capacitor [17]–[20], and static synchronous series compensator (SSSC) [21]–[26] are series FACTS devices and often connected in series with power transmission line. Series FACTS devices are equivalent to regulating the line impedance in grid and then controlling the line current and active power flow, but they are not able to control active and reactive power flow independently and simultaneously [1].

Unified power flow controller (UPFC) [27]–[33], shown in Fig. 1, is similar to the combination of a series SSSC and a shunt STATCOM, and can realize functions of shunt compensation, phase shifting, and series compensation, and control active and reactive power flow, respectively.

UPFC, STATCOM, and SSSC all contain big volume dc energy storage element, which usually results in high equipment failure rate, short life cycle, and high maintenance cost. In order to obtain a kind of device without dc energy storage element, the concept of virtual quadrature source was adopted [5]; a method for power flow control, i.e., ac–ac converter with controllable phase and amplitude (ACCPA), was presented [1], [34]–[36], which not only has the functions of voltage step-up and step-down, but also can regulate the phase angle of the output voltage lead or lag with respect to the input.

Both cascaded ACCPA [34], [35] and π model ACCPA [36] have a two-stage circuit structure, whose front stage is a buck-type ac converter (or unit) and is used to regulate the phase angle of its output voltage, and whose back stage is a boost-type ac converter (or unit) for regulating the amplitude of its output voltage with the front stage. The back stage only provides the function of voltage step-up for cascaded ACCPA and π model ACCPA. Prior to the use of two-stage ACCPA for power transmission in high-voltage grid, the problem of high-voltage stress should be solved first because power switches at present can only support limited voltage (much lower than that of high-voltage grid), even if multilevel ac converter [37] replaces two-level ac

Manuscript received December 11, 2018; revised March 24, 2019; accepted May 23, 2019. Date of publication June 2, 2019; date of current version November 12, 2019. This work was supported in part by the National Natural Science Foundation of China under Awards 51477107 and 51875380, in part by the Postdoctoral Science Foundation of China under Award 2015M571805, in part by the Postdoctoral Science Foundation of Jiangsu Province, China, under Award 1402107C, in part by the Open Research Funds of the Jiangsu Key Laboratory of Spectral Imaging & Intelligent Sense, Jiangsu Province, China, under Awards 3091801410402 and 3091801410408, and in part by the Fundamental Research Funds for the Central Universities under Award 30918014106. Recommended for publication by Associate Editor F. W. Fuchs. *(Corresponding author: Youjun Zhang.)*

Y. Zhang is with the School of Mechanical & Electrical Engineering, Soochow University, Suzhou 215021, China, and also with the Jiangsu Key Laboratory of Spectral Imaging & Intelligent Sense, and Ministerial Key Laboratory of JGMT, Nanjing University of Science and Technology, Nanjing 210016, China (e-mail: zhangyoujun@suda.edu.cn).

G. Lu and W. A. Khan are with the School of Mechanical & Electrical Engineering, Soochow University, Suzhou 215021, China (e-mail: 2453279086@qq.com; wajidkhanuet@ gmail.com).

Y. Zhang is with the Jiangsu Key Laboratory of Spectral Imaging & Intelligent Sense, Nanjing University of Science and Technology, Nanjing 210016, China (e-mail: olindazh@163.com).

Q. Zhu is with the School of Mechanical Engineering, Soochow University of Science and Technology, Suzhou 215009, China (e-mail: bob21cn@ 163.com).

Color versions of one or more of the figures in this paper are available online at http://ieeexplore.ieee.org.

Digital Object Identifier 10.1109/TPEL.2019.2920423

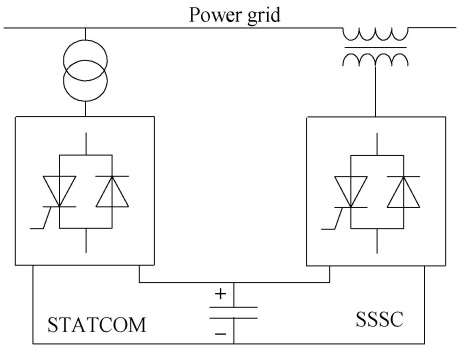

Fig. 1. Structure of UPFC.

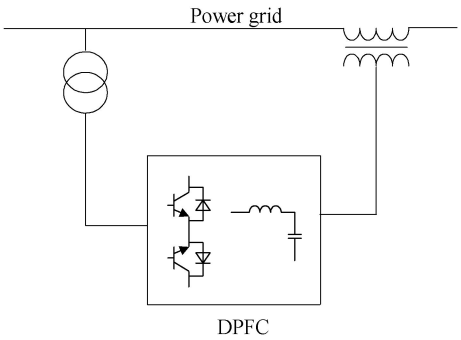

Fig. 2. Concept of DPFC.

converter in ACCPA. Taking into consideration the aforementioned problem, single-stage ACCPA [1] was developed, which introduces an output transformer to provide the function of voltage step-up and take the place of the boost-type ac converter (or unit) in two-stage ACCPA. Compared with two-stage ACCPA, single-stage ACCPA not only decreases the number of switching devices in circuit and reduces the complexity of system, but also decreases the number of power conversion stages (it usually means lower power loss and higher efficiency).

It is known that, if the phase and amplitude of the sending-end voltage in grid can be regulated, the effective control of active power flow and reactive power flow would be implemented [6]. For power transmission in grid, based on single-stage ACCPA, the concept of direct power flow controller (DPFC) was proposed, as shown in Fig. 2. DPFC does not contain dc energy storage element and has only one-stage conversion circuit. By connecting its regulated output compensation voltage with grid in series, DPFC is able to regulate the amplitude and phase angle of grid node voltage, respectively and simultaneously. The phase regulation range of output compensation voltage in DPFC is 360°. So, with respect to the original grid voltage, the regulated grid voltage can be controlled by DPFC to be step-up or step-down for its amplitude, and lead or lag for its phase angle. Thus, DPFC can effectively control active power flow and reactive power flow in grid separately. The topology structure and operational principle of DPFC were studied in detail. The regulation range of phase angle and amplitude of DPFC basic

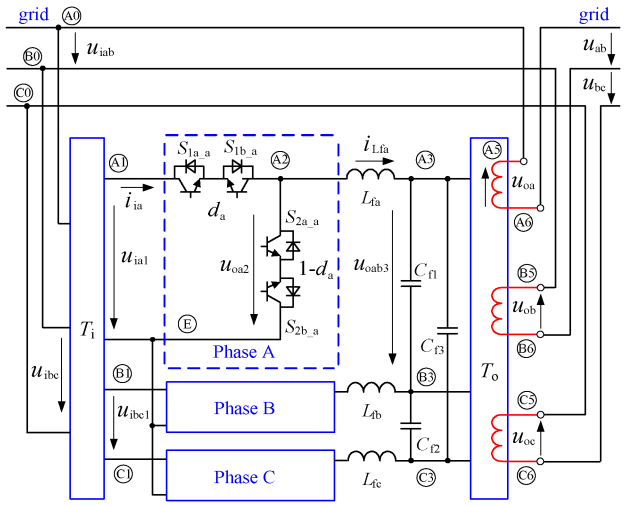

Fig. 3. Basic topology structure of DPFC.

circuit was described under 36 different combinations of connection groups of the input and output transformer. Experimental results of the prototype were shown to verify the feasibility of DPFC.

II. Direct Power Flow Controller

A. Topology Structure and Operational Principle

UPFC and the proposed DPFC are both for power flow control. Compared with UPFC, the proposed DPFC also has a parallel transformer and a series transformer, but has no dc energy storage element that easily leads to high equipment failure rate, short life cycle, and high maintenance cost. Furthermore, UPFC is similar to a two-stage conversion circuit, while DPFC has only one-stage conversion circuit. Usually, decreasing the number of power conversion stages is an effective method to achieve simpler structure, a smaller number of switching devices in circuit, higher stability, lower power loss, and higher efficiency.

Fig. 3 shows one of the DPFC basic circuits, whose three-phase input transformer $T_{\rm i}$ (or transformer group) is paralleled with grid, while the output voltage of three-phase output transformer $T_{\rm o}$ (or transformer group) is connected with grid in series. Three single-phase buck-type ac units and a three-phase output filter constitute its one-stage conversion circuit.

Assume that

1) original grid voltage is sinusoidal with angular frequency ω ($=2\pi f$, where f is its frequency);
2) circuit components are ideal;
3) as shown in Fig. 4, $T_{\rm i}$ is of Δ/Yn11-type connection group with turn ratio $N_{\rm i}$, and $T_{\rm o}$ is of Δ/Y1-type connection group with turn ratio $N_{\rm o}$ (note that points A5, B5, and C5 are not connected together, and the three secondary windings of $T_{\rm o}$ are separately connected with power transmission line in series);
4) low-frequency voltage drop across the inductor $L_{\rm fx}$ (x = a, b, c, where x is the name of phase in lowercase letter) is not taken into account.

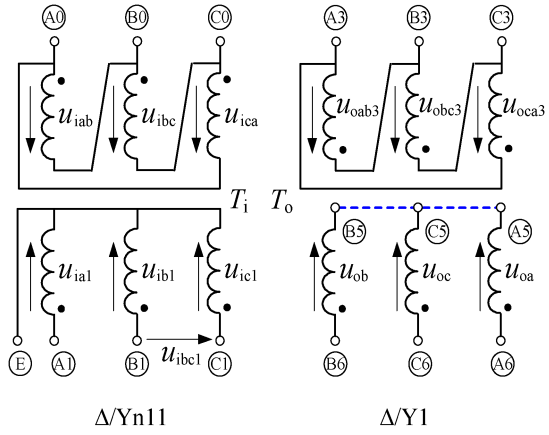

Fig. 4. Assumed connection groups.

If the original grid line voltages $u_{\rm iab}$, $u_{\rm ibc}$, $u_{\rm ica}$ and the duty ratio $d_{\rm x}$ are as below

$$\begin{cases} u_{\rm iab} = N_{\rm i}u_{\rm ia1} = U_{\rm imL}\ \sin\ \omega t \\ u_{\rm ibc} = N_{\rm i}u_{\rm ib1} = U_{\rm imL}\ \sin(\omega t - 120^\circ) \\ u_{\rm ica} = N_{\rm i}u_{\rm ic1} = U_{\rm imL}\ \sin(\omega t + 120^\circ) \end{cases} \tag{1}$$

$$\begin{cases} d_{\rm a} = k_0 + k_2 \sin(2\omega t + \beta_2) \\ d_{\rm b} = k_0 + k_2\ \sin[2(\omega t - 120^\circ) + \beta_2] \\ \quad = k_0 + k_2\ \sin(2\omega t + \beta_2 + 120^\circ) \\ d_{\rm c} = k_0 + k_2\ \sin[2(\omega t + 120^\circ) + \beta_2] \\ \quad = k_0 + k_2\ \sin(2\omega t + \beta_2 - 120^\circ) \end{cases} \tag{2}$$

where u_{ia1}, u_{ib1}, and u_{ic1} are the input voltages of three single-phase buck-type ac units, $U_{\rm imL}$ is the amplitude of $u_{\rm iab}$, β_2 is the initial phase angle of the ac component of $d_{\rm a}$ [5], and coefficients k_0 and k_2 are nonnegative, one knows that $k_2 \le k_0$ at $0 \le k_0 \le 0.5$, or $k_2 \le 1 - k_0$ at $0.5 \le k_0 \le 1$.

Delta (Δ)-type connection is adopted for capacitors of the three-phase output filter to cancel out the third harmonic voltages. After $L_{\rm fx}$ filters out the high-frequency component of u_{ox2} (output voltage of buck-type ac unit), the phase voltage u_{ox3} (between points X3 and E, not shown in Fig. 3, X = A, B, C, where X is the name of phase in uppercase letter) is output, then one can obtain the voltages u_{oab3}, u_{obc3}, u_{oca3}, $u_{\rm oa}$, $u_{\rm ob}$, and $u_{\rm oc}$ [1]

$$\begin{cases} u_{\rm oab3} = u_{\rm oa3} - u_{\rm ob3} = d_{\rm a}u_{\rm ia1} - d_{\rm b}u_{\rm ib1} \\ \quad = U_{\rm mL3}\ \sin\ (\omega t + \varphi_{\rm t}) \\ u_{\rm obc3} = u_{\rm ob3} - u_{\rm oc3} = d_{\rm b}u_{\rm ib1} - d_{\rm c}u_{\rm ic1} \\ \quad = U_{\rm mL3}\ \sin\ (\omega t + \varphi_{\rm t} - 120^\circ) \\ u_{\rm oca3} = u_{\rm oc3} - u_{\rm oa3} = d_{\rm c}u_{\rm ic1} - d_{\rm a}u_{\rm ia1} \\ \quad = U_{\rm mL3}\ \sin\ (\omega t + \varphi_{\rm t} + 120^\circ) \end{cases} \tag{3}$$

$$\begin{cases} u_{\rm oa} = \frac{U_{\rm mL3}}{N_{\rm o}}\ \sin\ (\omega t + \varphi_{\rm t} - 60^\circ) \\ u_{\rm ob} = \frac{U_{\rm mL3}}{N_{\rm o}}\ \sin\ (\omega t + \varphi_{\rm t} - 180^\circ) \\ u_{\rm oc} = \frac{U_{\rm mL3}}{N_{\rm o}}\ \sin\ (\omega t + \varphi_{\rm t} + 60^\circ) \end{cases} \tag{4}$$

$$\begin{cases} U_{\rm mL3} = \frac{\sqrt{3}k_0U_{\rm imL}}{N_{\rm i}}\sqrt{1 - \frac{k_2}{k_0}\ \sin\ \beta_2 + \frac{1}{4}\left(\frac{k_2}{k_0}\right)^2} \\ \varphi_{\rm t} = \arctan\ \frac{(k_2/k_0)\cos\ \beta_2}{2-(k_2/k_0)\sin\ \beta_2} + 30^\circ \end{cases} \tag{5}$$

where U_{mL3} is the amplitude of u_{oab3} with phase angle $\varphi_{\rm t}$. In positive sequence, a phase difference of 120° is present among u_{oab3}, u_{obc3}, and u_{oca3} (or $u_{\rm oa}$, $u_{\rm ob}$, and $u_{\rm oc}$).

The regulated grid line voltages ($u_{\rm ab}$, $u_{\rm bc}$, and $u_{\rm ca}$) are

$$\begin{cases} u_{\rm ab} = u_{\rm iab} + (u_{\rm oa} - u_{\rm ob}) = u_{\rm iab} + u_{\rm oab} \\ \quad = u_{\rm iab} + \Delta u_{\rm ab} = U_{\rm mL}\ \sin\ (\omega t + \varphi_{\rm r}) \\ u_{\rm bc} = u_{\rm ibc} + (u_{\rm ob} - u_{\rm oc}) = u_{\rm ibc} + u_{\rm obc} \\ \quad = u_{\rm ibc} + \Delta u_{\rm bc} = U_{\rm mL}\ \sin\ (\omega t + \varphi_{\rm r} - 120^\circ) \\ u_{\rm ca} = u_{\rm ica} + (u_{\rm oc} - u_{\rm oa}) = u_{\rm ica} + u_{\rm oca} \\ \quad = u_{\rm ica} + \Delta u_{\rm ca} = U_{\rm mL}\ \sin\ (\omega t + \varphi_{\rm r} + 120^\circ) \end{cases} \tag{6}$$

$$\begin{cases} u_{\rm oab} = \Delta u_{\rm ab} = U_{\rm omL}\ \sin\ (\omega t + \varphi_{\rm o}) \\ \quad = \frac{\sqrt{3}U_{\rm mL3}}{N_{\rm o}}\ \sin\ (\omega t + \varphi_{\rm t} - 30^\circ) \\ u_{\rm obc} = \Delta u_{\rm bc} = \frac{\sqrt{3}U_{\rm mL3}}{N_{\rm o}}\ \sin\ (\omega t + \varphi_{\rm t} - 150^\circ) \\ u_{\rm oca} = \Delta u_{\rm ca} = \frac{\sqrt{3}U_{\rm mL3}}{N_{\rm o}}\ \sin\ (\omega t + \varphi_{\rm t} + 90^\circ) \end{cases} \tag{7}$$

where $U_{\rm mL}$ and $\varphi_{\rm r}$ are the amplitude and phase angle of $u_{\rm ab}$, and we define $u_{\rm oab} = u_{\rm oa} - u_{\rm ob} = \Delta u_{\rm ab}$, $u_{\rm obc} = u_{\rm ob} - u_{\rm oc} = \Delta u_{\rm bc}$, and $u_{\rm oca} = u_{\rm oc} - u_{\rm oa} = \Delta u_{\rm ca}$. Apparently, $u_{\rm ox}$ is the compensation phase voltage of grid, while $u_{\rm oab}$ ($\Delta u_{\rm ab}$), $u_{\rm obc}$ ($\Delta u_{\rm bc}$), and $u_{\rm oca}$ ($\Delta u_{\rm ca}$) are the compensation line voltages of grid ($\varphi_{\rm o}$ is the phase angle of $u_{\rm oab}$ with amplitude $U_{\rm omL}$).

Here, $\varphi_{\rm o}$, $U_{\rm omL}$, $\varphi_{\rm r}$, and $U_{\rm mL}$ would be given as

$$\varphi_{\rm o} = \varphi_{\rm t} - 30^\circ = \arctan\ \frac{(k_2/k_0)\cos\ \beta_2}{2 - (k_2/k_0)\sin\ \beta_2} \tag{8}$$

$$U_{\rm omL} = \frac{3k_0U_{\rm imL}}{N_{\rm i}N_{\rm o}}\sqrt{1 - \frac{k_2}{k_0}\ \sin\ \beta_2 + \frac{1}{4}\left(\frac{k_2}{k_0}\right)^2} \tag{9}$$

$$\varphi_{\rm r} = \arctan\ \frac{U_{\rm omL}\ \sin\ \varphi_{\rm o}}{U_{\rm imL} + U_{\rm omL}\ \cos\ \varphi_{\rm o}} \tag{10}$$

$$U_{\rm mL} = \sqrt{(U_{\rm imL} + U_{\rm omL}\ \cos\ \varphi_{\rm o})^2 + (U_{\rm omL}\ \sin\ \varphi_{\rm o})^2}. \tag{11}$$

From (8)–(11) we know that $\varphi_{\rm o}$ of the grid compensation line voltage $u_{\rm oab}$ ($\Delta u_{\rm ab}$) is controlled by two parameters (k_2/k_0 and β_2), $U_{\rm omL}$ is controlled by three parameters (k_0, k_2/k_0, and β_2), and so are $U_{\rm mL}$ and $\varphi_{\rm r}$.

B. Range of the Grid Compensation Voltage

From (6), (10), and (11), one knows that the phase angle $\varphi_{\rm r}$ and the amplitude $U_{\rm mL}$ of the regulated grid voltage are dependent on the range of grid compensation voltage.

With the change of k_2/k_0 (letting $\alpha = k_2/k_0$, $0 \le \alpha \le 1$, $0 \le k_0 \le 1/(1+\alpha) \le 1$), the maximum and minimum

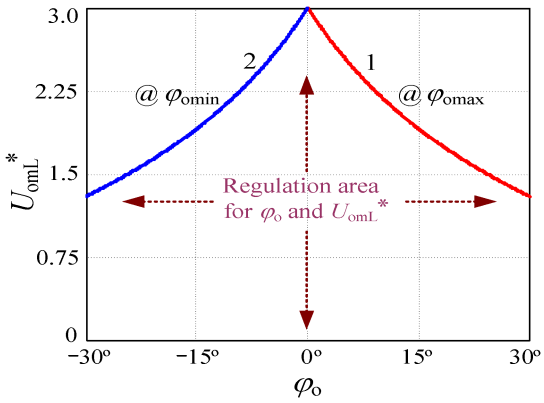

Fig. 5. Regulation range of U_{omL}^* and φ_{o}.

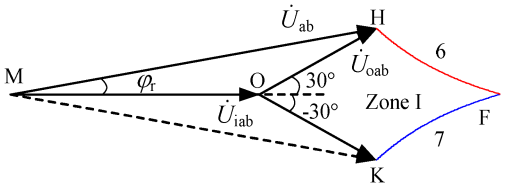

Fig. 6. Basic regulation zone I of DPFC.

of φ_{o} would, respectively, be

$$\begin{cases} \varphi_{\mathrm{omax}} = arcsin\frac{\alpha}{2} = \beta_2, & \beta_2 \in [0°, 90°] \\ \varphi_{\mathrm{omin}} = -arcsin\frac{\alpha}{2} = \beta_2 - 180°, & \beta_2 \in (90°, 180°]. \end{cases} \tag{12}$$

The regulation range of φ_{o} would increase from zero (at $\alpha = 0$) to [−30°, 30°] (at $\alpha = 1$) with the increase of α. Known from (12), there would be $0 \le \sin\beta_2 = 0.5\alpha \le 0.5$ if φ_{o} is equal to extremum. It indicates that $\beta_2 \in [0°, 30°]$ or $[150°, 180°]$ in the range of 0–360°.

According to (9) and (12), one knows that

$$0 \le U_{\mathrm{omL}}^* = N_{\mathrm{i}}N_{\mathrm{o}}\frac{U_{\mathrm{omL}}}{U_{\mathrm{imL}}} \le \frac{3}{1+\alpha}\sqrt{1-\frac{1}{4}\alpha^2}. \tag{13}$$

At extremum of φ_{o}, with the increase of α (k_2/k_0) the regulation range of U_{omL}^* ($N_{\mathrm{i}}N_{\mathrm{o}}U_{\mathrm{omL}}/U_{\mathrm{imL}}$) decreases.

Substituting (12) into (13), we have

$$0 \le U_{\mathrm{omL}}^* \le \frac{3}{1+2\left|\sin\varphi_{\mathrm{oext}}\right|}\sqrt{1-\left(\sin\varphi_{\mathrm{oext}}\right)^2} \tag{14}$$

where φ_{oext} is the extremum of φ_{o}. As shown in Fig. 5, the regulation range of φ_{o} and that of U_{omL}^* form a regulation area [1]. Curve 1 shows the maximum of U_{omL}^* at φ_{omax}, while curve 2 shows the maximum of U_{omL}^* at φ_{omin}.

According to Fig. 5, one can obtain Fig. 6, in which zone I (O–H–F–K) is the regulation area for U_{omL} and φ_{o} of the compensation grid voltage, the same as that in Fig. 5 (note that there is a different coordinate system). Zone I is the basic regulation zone of DPFC. Here, with respect to the original grid voltage u_{iab}, the phase angle φ_{r} of the regulated grid voltage u_{ab} can be regulated lead or lag, but its regulated amplitude U_{mL} can only become larger than the amplitude U_{imL} of u_{iab}. If we want to regulate U_{mL} to be smaller than U_{imL}, it is necessary to research on other basic regulation zones of DPFC.

III. Full Regulation Zone With 360° Range

A. Different Combinations of Connection Groups of Transformers

As shown in Figs. 5 and 6, when T_{i} is of Δ/Yn11-type connection group and T_{o} is of Δ/Y1-type connection group, the regulation range of φ_{o} is [−30°, 30°] and the maximum of U_{omL}^* is 3. Obviously, if the connection groups of T_{i} and T_{o} are changed, the phase angle and amplitude of the compensation grid voltage and the regulated grid voltage will be slightly changed from (8), (9), (10), and (11), respectively.

It is necessary to adopt the input connection of T_{i} with Δ type to prevent third harmonic current from flowing into the grid. The output connection of T_{i} should be Y type with neutral line to provide input voltages for three single-phase buck-type ac units. Similarly, Δ type is adopted for the capacitors of the three-phase output filter and the input connection of T_{o}, to cancel out third harmonic voltage. For connecting the output voltage of T_{o} with grid in series, only Y type is suitable for the output connection of T_{o} (note that its three secondary windings are not connected together).

Six types of connection groups (Δ/Yn1, Δ/Yn3, Δ/Yn5, Δ/Yn7, Δ/Yn9, and Δ/Yn11) are suitable for input transformer T_{i}, as shown in Fig. 7. For output transformer T_{o}, there are also six suitable types of connection groups (Δ/Y1, Δ/Y3, Δ/Y5, Δ/Y7, Δ/Y9, and Δ/Y11), as shown in Fig. 8. Thus, DPFC has at least 36 different combinations of connection groups of the input and output transformer.

Table I shows the regulation range of phase angle φ_{o} for each kind of combination. Totally, there are six ranges, [−30°, 30°], [30°, 90°], [90°, 150°], [150°, 210°], [210°, 270°], and [−90°, −30°], corresponding to zone I, zone II (O–H–L–G, as shown in Fig. 9), zone III (O–G–J–P), zone IV (O–P–Q–R), zone V (O–R–U–V), and zone VI (O–V–W–K), respectively. The maximum of U_{om}^* of each zone is 3.

For example, if T_{i} is kept as of Δ/Yn11-type connection group and T_{o} is changed to Δ/Y9 type, the regulation area for φ_{o} (comparing (16) and (8), the compensation line voltage phase angle φ_{o} has increased by 120° while moving from zone I to zone III) and U_{omL} of compensation grid voltage is in zone III (O–G–J–P), where it shows that

$$\dot{U}_{\mathrm{ab}} = \dot{U}_{\mathrm{iab}} + \dot{U}_{\mathrm{oab}} \tag{15}$$

$$\varphi_{\mathrm{o}} = (\varphi_{\mathrm{t}} - 30°) + 120° = 120° + \arctan\frac{(k_2/k_0)\cos\beta_2}{2-(k_2/k_0)\sin\beta_2}. \tag{16}$$

From (8) and (16), Table I, and Fig. 9, according to the number of connection groups of T_{i} and T_{o}, one obtains a general equation of φ_{o} for all the zones

$$\varphi_{\mathrm{o}} = \varphi_{\mathrm{t}} - 30° - (n_{\mathrm{i}} + n_{\mathrm{o}}) \times 30° \tag{17}$$

where n_{i} is the number of connection groups of T_{i}, and n_{o} is that of T_{o}.

TABLE I
REGULATION RANGE OF φ_o FOR 36 DIFFERENT COMBINATIONS

The regulation range of φ_o/°		T_i					
		Δ/Yn11	Δ/Yn9	Δ/Yn7	Δ/Yn5	Δ/Yn3	Δ/Yn1
T_o	Δ/Y1	[–30°, 30°]	[30°, 90°]	[90°, 150°]	[150°, 210°]	[210°, 270°]	[–90°, -30°]
	Δ/Y3	[–90°, -30°]	[–30°, 30°]	[30°, 90°]	[90°, 150°]	[150°, 210°]	[210°, 270°]
	Δ/Y5	[210°, 270°]	[–90°, -30°]	[–30°, 30°]	[30°, 90°]	[90°, 150°]	[150°, 210°]
	Δ/Y7	[150°, 210°]	[210°, 270°]	[–90°, -30°]	[–30°, 30°]	[30°, 90°]	[90°, 150°]
	Δ/Y9	[90°, 150°]	[150°, 210°]	[210°, 270°]	[–90°, -30°]	[–30°, 30°]	[30°, 90°]
	Δ/Y11	[30°, 90°]	[90°, 150°]	[150°, 210°]	[210°, 270°]	[–90°, -30°]	[–30°, 30°]

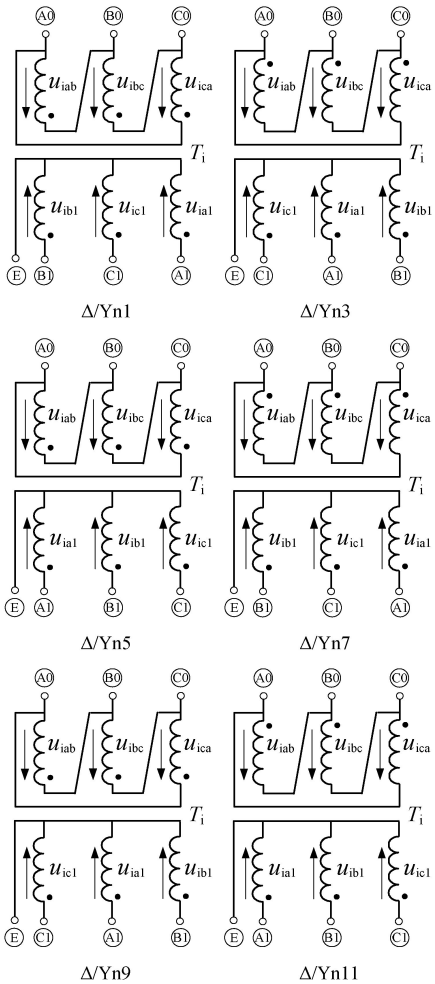

Fig. 7. Six suitable connection groups for T_i.

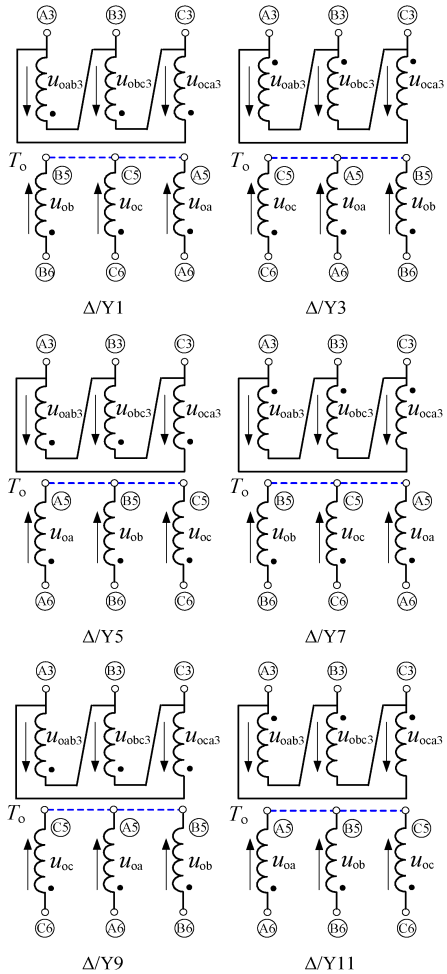

Fig. 8. Six suitable connection groups for T_o.

Then, the regulation range of φ_o is

$$-30^\circ-(n_i+n_o)\times 30^\circ \le \varphi_o \le 30^\circ-(n_i+n_o)\times 30^\circ. \tag{18}$$

B. DPFC With Full 360° Regulation Zone

Comparing Figs. 6 and 9, one knows that DPFC would have a full 360° regulation zone for compensation line voltages (u_{oab}, u_{obc}, and u_{oca}) of grid if six basic regulation zones can be combined. It means that the regulation area of voltage u_{ab} in Fig. 9 is six times of that in Fig. 6. So, in Fig. 9, with respect to the original grid voltage u_{iab}, not only the phase angle φ_r of the regulated grid voltage u_{ab} can be regulated lead or lag, but also its regulated amplitude U_{mL} can become larger or smaller than the amplitude U_{imL} of u_{iab}.

DPFC with full 360° regulation zone is shown in Fig. 10, where two selection switches (S_{Gi} and S_{Go}) are added based on the topology structure shown in Fig. 3. S_{Gi} has three selection modes, while S_{Go} has two modes.

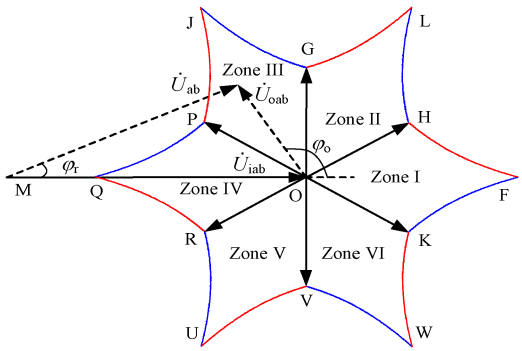

Fig. 9. Six basic regulation zones of DPFC.

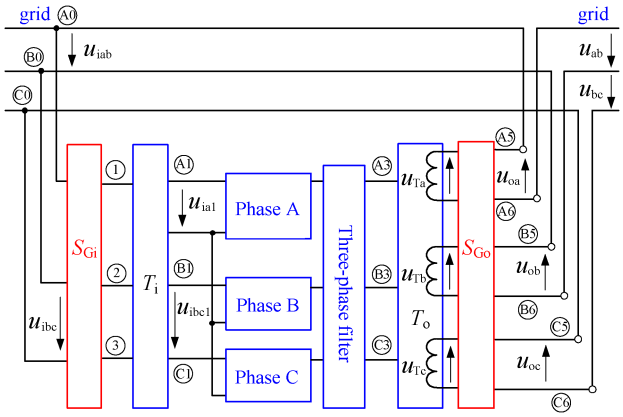

Fig. 10. DPFC with full 360° regulation zone.

TABLE II
REGULATION RANGE OF φ_o IN DPFC

S_{Gi} mode	S_{Go} mode	Zone	Range of φ_o
First	First	I	[–30°, 30°]
Second	First	III	[90°, 150°]
Third	First	V	[210°, 270°]
First	Second	IV	[150°, 210°]
Second	Second	VI	[–90°, -30°]
Third	Second	II	[30°, 90°]

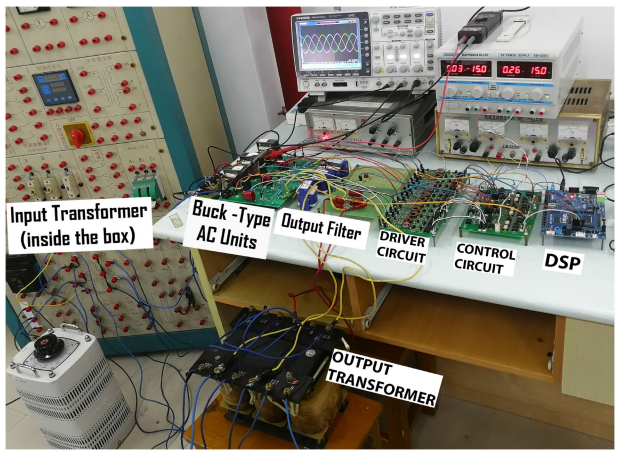

Fig. 11. DPFC prototype.

Say, the first mode of S_{Gi} is to connect point A0 with point 1, point B0 with point 2, and point C0 with point 3. The second mode of S_{Gi} is to connect point A0 with point 2, point B0 with point 3, and point C0 with point 1. The third mode of S_{Gi} is to connect point A0 with point 3, point B0 with point 1, and point C0 with point 2. The first mode of S_{Go} is to let $u_{oa} = u_{Ta}$, $u_{ob} = u_{Tb}$, and $u_{oc} = u_{Tc}$, where u_{Ta}, u_{Tb}, and u_{Tc} are the output phase voltages of T_o. The second mode of S_{Go} is to let $u_{oa} = -u_{Ta}$, $u_{ob} = -u_{Tb}$, and $u_{oc} = -u_{Tc}$.

If assuming T_i is of Δ/Yn11-type connection group under the first mode of S_{Gi}, then T_i is of Δ/Yn7 type under the second mode of S_{Gi}, and of Δ/Yn3 type under the third mode of S_{Gi}. If assuming T_o is of Δ/Y1-type connection group under the first mode of S_{Go}, then T_o is of Δ/Y7 type under the second mode of S_{Go}.

Apparently, under different combination modes of S_{Gi} and S_{Go}, compensation grid voltages can be regulated in a different zone, as shown in Table II. There are six different combination modes of selection switches that lead to six different zones; thus, DPFC has full 360° regulation zone for compensation of grid voltages.

Selection switch S_{Gi} can also be added after the secondary windings of input transformer T_i, where S_{Gi} has two selection modes to change the input voltage direction of each single-phase buck-type ac unit (for instance, if T_i is of Δ/Yn11-type connection group under the first mode of S_{Gi}, then T_i is of Δ/Yn5 type under the second mode of S_{Gi}), while selection switch S_{Go} can be added in front of the primary windings of output transformer T_o, where S_{Go} has three selection modes to change the connection group of T_o (for instance, if T_o is of Δ/Y1-type connection group under the first mode of S_{Go}, then T_o is of Δ/Y9 type under the second mode of S_{Go}, and T_o is of Δ/Y5 type under the third mode of S_{Go}).

Here, S_{Gi} has two selection modes, while S_{Go} has three modes. According to connection group of the input and output transformer, from Table I we know that 1) when S_{Gi} is under the first mode, the regulation area of DPFC is zones I, III, and V, corresponding to the first, second, and third modes of S_{Go}, respectively; and 2) when S_{Gi} is under the second mode, the regulation area of DPFC is zones IV, VI, and II, corresponding to the first, second, and third modes of S_{Go}, respectively.

There are other four options to place S_{Gi} and S_{Go}. Option 1 is that S_{Gi} is added before the primary windings of T_i and S_{Go} is added after the secondary windings of T_i. Option 2 is that S_{Gi} and S_{Go} are added before the primary windings of T_i and T_o, respectively. Option 3 is that S_{Gi} is added before the primary windings of T_o and S_{Go} is added after the secondary windings of T_o. Option 4 is that S_{Gi} and S_{Go} are added after the secondary windings of T_i and T_o, respectively.

IV. EXPERIMENTAL RESULTS

A prototype shown in Fig. 11 was manufactured, and experiments were performed for different transformer connection groups (the connection groups are changed manually; selection

TABLE III
EXPERIMENTAL SPECIFICATIONS

specification	value
amplitude of original grid line voltage: U_{imL}	$200\sqrt{2}$ V
frequency of grid voltage: f	50 Hz
switching frequency: f_s	22.5 kHz
turn ratio of the input transformer T_i: N_i	200/121
turn ratio of the output transformer T_o: N_o	220/130
output filter inductance: L_{fa}=L_{fb}=L_{fc}	0.52 mH
output filter capacitor: C_{f1}=C_{f2}=C_{f3}	6.6 μF
switch device	IRFP460A
DSP IC	TMS320F2812

switch will be discussed in further work) to verify the feasibility of DPFC. Table III lists its specifications.

When T_i is of Δ/Yn11-type connection group while T_o is of Δ/Y1 (regulation area is zone I), $k_0 = 0.500$, $k_2 = 0.419$, and $\beta_2 = 24.8°$, Fig. 12 shows the experimental waveforms of DPFC in zone I.

For phase A buck-type ac unit in DPFC, its input voltage u_{ia1} and its output voltages u_{oa2} and u_{oa3} (between points A3 and E in Fig. 3) are shown in Fig. 12(a). Here, u_{ia1} is modulated by phase A buck-type ac unit with duty ratio d_a, u_{oa2} is a high-frequency pulse sequence, and u_{ia1} is its envelope curve. After most of the high-frequency components of u_{oa2} are filtered out by L_{fa}, u_{oa3} is obtained, which has not only fundamental voltage component, but also third harmonic voltage component and a small amount of high-frequency components.

The experimental waveforms of u_{oa3}, u_{ob3} (between points B3 and E in Fig. 3), u_{oab3} (the voltage across capacitor C_{f1}), and u_{oa} (phase A compensation voltage of grid) are shown in Fig. 12(b). u_{ob3}, the output voltage of phase B buck-type ac unit after the inductor L_{fb}, is similar to u_{oa3} but lags it by 120° at fundamental frequency. u_{oc3} (between points C3 and E in Fig. 3, but not shown in Fig. 12(b)), the output voltage of phase C buck-type ac unit after the inductor L_{fc}, is also similar to u_{oa3} but leads it by 120° at fundamental frequency. We know that $u_{oab3} = (u_{oa3} - u_{ob3})$, which is the voltage between points A3 and B3, and in theory only contains fundamental voltage, because the third harmonic voltage components in u_{oa3} and u_{ob3} cancel each other out, and capacitor C_{f1} filters off their high-frequency voltage components. Known from Figs. 8 and 12(b), u_{oa} lags u_{oab3} by $-60°$.

The experimental waveforms of the original grid line voltage u_{iab} (namely, input line voltage of DPFC), u_{oa}, u_{ob} (phase B compensation voltage of grid, lagging u_{oa} by 120°), and the regulated grid line voltage u_{ab} (where $u_{ab} = u_{iab} + u_{oa} - u_{ob}$) are shown in Fig. 12(c). u_{iab} is compensated by u_{oa} and u_{ob} to obtain u_{ab}, which has different phase and amplitude from u_{iab}. With the help of Code Composer Studio software and a DSP emulator, it is easy to watch variables. One can measure that in Fig. 12(c) u_{ab} is leading u_{iab} by phase angle φ_r of 7.99° and has an amplitude U_{mL} of $295\sqrt{2}$ V larger than that of u_{iab}

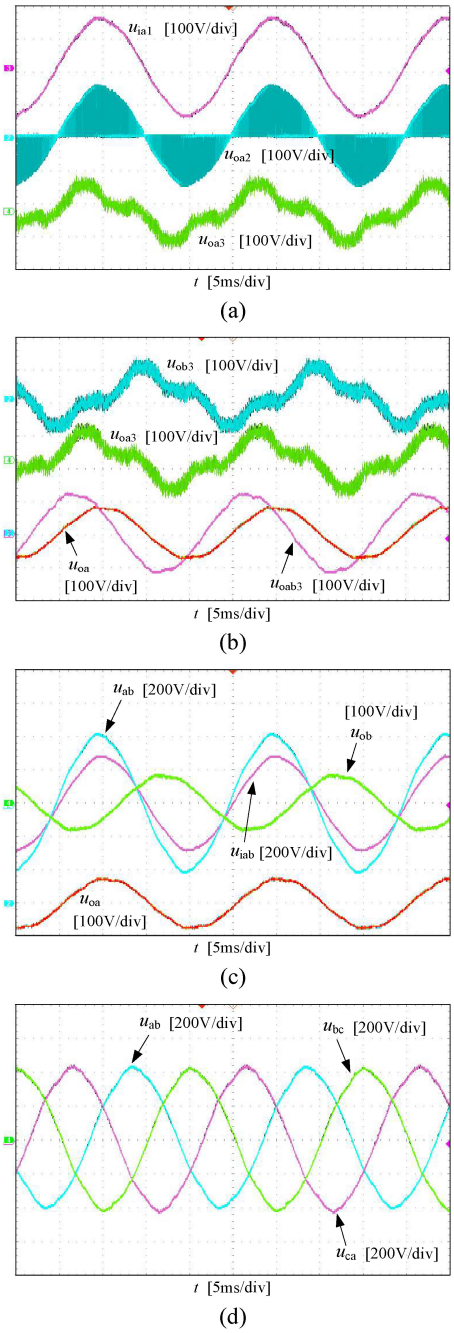

Fig. 12. Experimental waveforms of DPFC at zone I when $k_0 = 0.500$, $k_2 = 0.419$, and $\beta_2 = 24.8°$. (a) u_{ia1}, u_{oa2}, and u_{oa3}. (b) u_{oa3}, u_{ob3}, and u_{oab3}. (c) u_{iab}, u_{oa}, u_{ob}, and u_{ab}. (d) u_{ab}, u_{bc}, and u_{ca}.

(the measured values are almost the same as calculated values of 8.07° and $292\sqrt{2}$ V, respectively). As we can see, with open-loop control, the difference between the measured value and the calculated value is very small. It verifies the correctness of theoretical analysis of DPFC.

The experimental waveforms of the regulated grid line voltages u_{ab}, u_{bc} ($u_{bc} = u_{ibc} + u_{ob} - u_{oc}$), and u_{ca} ($u_{ca} = u_{ica} + u_{oc} - u_{oa}$) are shown in Fig. 12(d). With a phase difference of 120°, u_{ab}, u_{bc}, and u_{ca} are symmetrical in positive sequence (usually the original grid line voltages u_{iab}, u_{ibc}, and u_{ica} are symmetrical, which clearly means that the

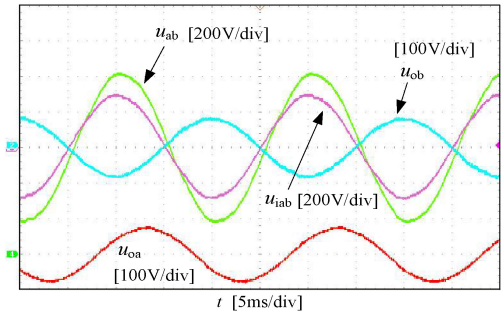

Fig. 13. Experimental waveforms of DPFC at zone I when $k_0 = 0.500$, $k_2 = 0.419$, and $\beta_2 = -24.8°$.

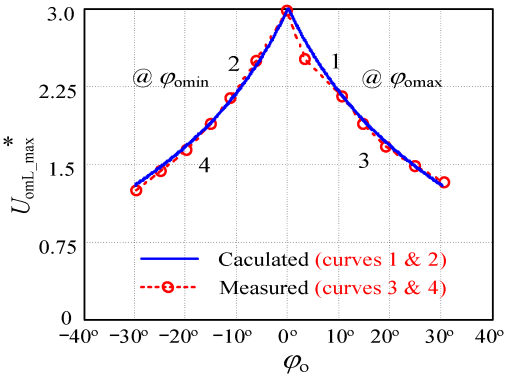

Fig. 14. Measured maximum U^*_{omL} and φ_{omax} or φ_{omin}.

compensation phase voltages u_{oa}, u_{ob}, and u_{oc} must be symmetrical).

While $k_0 = 0.500$, $k_2 = 0.419$, $\beta_2 = -24.8°$, and regulation area is zone I, the experimental waveforms of u_{iab}, u_{oa}, u_{ob}, and u_{ab} are shown in Fig. 13, where u_{ab} lags u_{iab} by $-8.10°$ and has an amplitude of $296\sqrt{2}$ V larger than that of u_{iab} (the measured values are almost the same as calculated values of $-8.07°$ and $292\sqrt{2}$ V, respectively).

We know that, for obtaining the desired regulated grid line voltage u_{ab} (or u_{bc} and u_{ca}), the compensation line voltage of grid Δu_{ab} ($\Delta u_{ab} = u_{oab} = u_{oa} - u_{ob}$, $\Delta u_{bc} = u_{obc} = u_{ob} - u_{oc}$, and $\Delta u_{ca} = u_{oca} = u_{oc} - u_{oa}$) should be controlled. When T_i is of Δ/Yn11-type connection group and T_o is of Δ/Y1 type (u_{oab}, u_{obc}, and u_{oca} can be measured easily when points A5, B5, and C5 are connected together while the three secondary windings of the output transformer T_o are not connected to the grid), the measurement results (the maximum of U^*_{omL} and φ_{omax} or φ_{omin}) are shown in Fig. 14.

Curves 3 and 1 in Fig. 14 show the measured and calculated φ_{omax} and the maximum of U^*_{omL}, respectively. While curves 4 and 2 show the measured and calculated φ_{omin} and the maximum of U^*_{omL}, respectively. The measured regulation area of the phase angle φ_o and the amplitude U^*_{omL} of u_{oab} is covered by curves 3 and 4. (The calculated regulation area of φ_o and U^*_{omL} is covered by curves 1 and 2.)

While T_i is of Δ/Yn3-type connection group and T_o is of Δ/Y7 type (regulation area is zone II), $k_0 = 0.500$, $k_2 = 0.419$, and $\beta_2 = 24.8°$, the experimental waveforms of the original grid line voltage u_{iab}, the grid compensation phase voltages u_{oa} and u_{ob}, and the regulated grid line voltage u_{ab} are shown in Fig. 15,

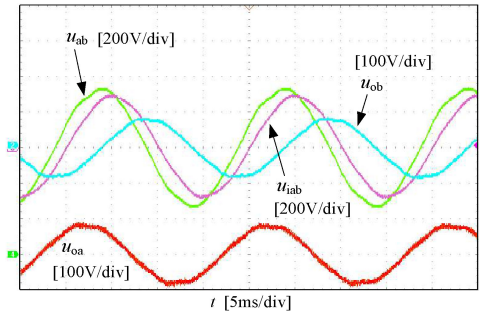

Fig. 15. Experimental waveforms of DPFC at zone II when $k_0 = 0.500$, $k_2 = 0.419$, and $\beta_2 = 24.8°$.

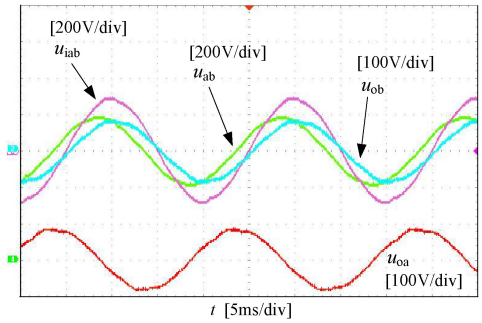

Fig. 16. Experimental waveforms of DPFC at zone III when $k_0 = 0.500$, $k_2 = 0.419$, and $\beta_2 = 24.8°$.

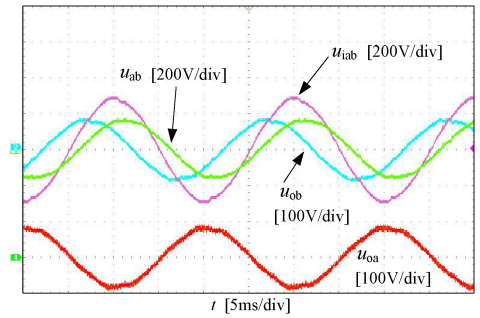

Fig. 17. Experimental waveforms of DPFC at zone IV when $k_0 = 0.500$, $k_2 = 0.419$, and $\beta_2 = 24.8°$.

where u_{ab} is leading u_{iab} by 24.97° and has an amplitude of $237\sqrt{2}$ V larger than that of u_{iab} (the measured values are almost the same as calculated values of 24.94° and $233\sqrt{2}$ V, respectively).

While T_i is of Δ/Yn7-type connection group and T_o is of Δ/Y1 type (regulation area is zone III), $k_0 = 0.500$, $k_2 = 0.419$, and $\beta_2 = 24.8°$, the experimental waveforms of u_{iab}, u_{oa}, u_{ob}, and u_{ab} are shown in Fig. 16, where u_{ab} is leading u_{iab} by 25.11° and has an amplitude of $133\sqrt{2}$ V smaller than that of u_{iab} (the calculated values are 25.06° and $131\sqrt{2}$ V, respectively, which are almost the same as measured values).

While T_i is of Δ/Yn11-type connection group and T_o is of Δ/Y7 type (regulation area is zone IV), $k_0 = 0.500$, $k_2 = 0.419$, and $\beta_2 = 24.8°$, the experimental waveforms of u_{iab}, u_{oa}, u_{ob}, and u_{ab} are shown in Fig. 17, where u_{ab} lags u_{iab} by $-21.19°$ and has an amplitude of $114\sqrt{2}$ V smaller than that of u_{iab} (the calculated values are $-20.16°$ and $112\sqrt{2}$ V, respectively, which are very close to the measured values).

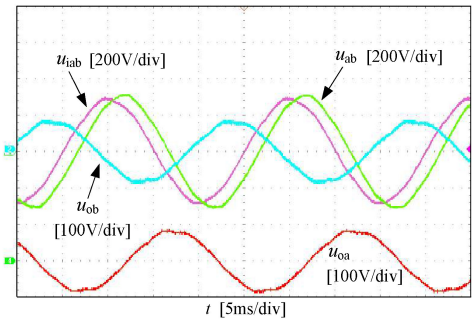

Fig. 18. Experimental waveforms of DPFC at zone V when $k_0 = 0.500$, $k_2 = 0.419$, and $\beta_2 = 24.8°$.

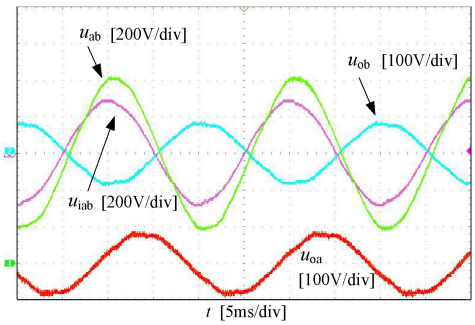

Fig. 19. Experimental waveforms of DPFC at zone VI when $k_0 = 0.500$, $k_2 = 0.419$, and $\beta_2 = 24.8°$.

While T_i is of Δ/Yn3-type connection group and T_o is of Δ/Y1 type (regulation area is zone V), $k_0 = 0.500$, $k_2 = 0.419$, and $\beta_2 = 24.8°$, the experimental waveforms of u_{iab}, u_{oa}, u_{ob}, and u_{ab} are shown in Fig. 18, where u_{ab} lags u_{iab} by $-26.74°$ and has an amplitude of $225\sqrt{2}$ V larger than that of u_{iab} (the calculated values are $-26.94°$ and $222\sqrt{2}$ V, respectively, which are almost the same as measured values).

While T_i is of Δ/Yn7-type connection group and T_o is of Δ/Y7 type (regulation area is zone VI), $k_0 = 0.500$, $k_2 = 0.419$, and $\beta_2 = 24.8°$, the experimental waveforms of u_{iab}, u_{oa}, u_{ob}, and u_{ab} are shown in Fig. 19, where u_{ab} lags u_{iab} by $-11.50°$ and has an amplitude of $293\sqrt{2}$ V larger than that of u_{iab} (the measured values are almost the same as calculated values of $-11.37°$ and $290\sqrt{2}$ V, respectively).

V. Conclusion

For power transmission in grid, a new concept of DPFC was proposed on the basis of single-stage ACCPA. Similar to UPFC, DPFC also has a parallel transformer and a series transformer but has only one-stage conversion circuit and has no dc energy storage element that usually results in high failure rate. By connecting its regulated output compensation voltage with grid in series, DPFC is able to regulate the amplitude and phase angle of grid node voltage, respectively and simultaneously. Thus, DPFC can effectively control active power flow and reactive power flow in grid separately.

The basic circuit structure of DPFC is simple, and only consists of three single-phase buck-type ac units with a three-phase output filter. With respect to the input voltage of DPFC basic circuit, the phase regulation width of its output voltage is 60°, which is easy to extend to 360° with two groups of selection switches that change the connection groups of the input transformer and output transformer. The experimental results of the prototype showed its feasibility and verified the theoretical analysis of DPFC.

References

[1] Y. Zhang, S. Guan, and Y. Zhang, "Single-stage ac–ac converter with controllable phase and amplitude," *IEEE Trans. Power Electron.*, vol. 34, no. 7, pp. 6991–7000, Jul. 2019.

[2] H. Acikgoz, O. F. Kececioglu, A. Gani, M. Tekin, and M. Sekkeli, "Robust control of shunt active power filter using interval type-2 fuzzy logic controller for power quality improvement (robusno reguliranje usporedno aktivnog filtra snage pomocu regulatora neizrazite logike intervala tipa-2 za poboljsanje kvalitete energije)," *Teh. Vjesn.-Tech. Gaz.*, vol. 24, no. S2, pp. 363–369, 2017.

[3] O. F. Kececioglu, H. Acikgoz, and M. Sekkeli, "Advanced configuration of hybrid passive filter for reactive power and harmonic compensation," *SpringerPlus*, vol. 5, no. 1, p. 1228, 2016.

[4] O. F. Kececioglu, H. Acikgoz, C. Yildiz, A. Gani, and M. Sekkeli, "Power quality improvement using hybrid passive filter configuration for wind energy systems," *J. Elect. Eng. Technol.*, vol. 12, no. 1, pp. 207–216, 2017.

[5] D. M. Divan and J. Sastry, "Voltage synthesis using dual virtual quadrature sources—A new concept in ac power conversion," *IEEE Trans. Power Electron.*, vol. 23, no. 6, pp. 3004–3013, Nov. 2008.

[6] K. K. Sen and M. L. Sen, "Introducing the family of "Sen" transformers: A set of power flow controlling transformers," *IEEE Trans. Power Del.*, vol. 18, no. 1, pp. 149–157, Jan. 2003.

[7] M. S EI-Moursi and A. M. Sharaf, "Novel reactive power controllers for the STATCOM and SSSC," *Elect. Power Syst. Res.*, vol. 76, no. 4, pp. 228–241, Jan. 2006.

[8] B. Gultekin *et al.*, "Design and implementation of a 154-kV $\pm$ 50-Mvar transmission STATCOM based on 21-level cascaded multilevel converter," *IEEE Trans. Ind. Appl.*, vol. 48, no. 3, pp. 1030–1045, May/Jun. 2012.

[9] J. C. Das, "Application of STATCOM to an industrial distribution system connected to a weak utility system," in *Proc. IEEE Pulp, Paper Forest Ind. Conf.*, 2016, pp. 124–135.

[10] L. Wang, C. Lam, and M. Wong, "A hybrid-STATCOM with wide compensation range and low dc-link voltage," *IEEE Trans. Ind. Electron.*, vol. 63, no. 6, pp. 3333–3343, Jun. 2016.

[11] B. Gultekin and M. Ermis, "Cascaded multilevel converter-based transmission STATCOM: System design methodology and development of a 12 kV $\pm$ 12 MVAr power stage," *IEEE Trans. Power Electron.*, vol. 28, no. 11, pp. 4930–4950, Nov. 2013.

[12] S. Das, D. Chatterjee, and S. K. Goswami, "Optimisation-based improved switching technique for static VAr compensator considering minimum source harmonic injection," *IET Power Electron.*, vol. 9, no. 7, pp. 1362–1373, Jun. 2016.

[13] J. H. Tovar-Hernandez, C. R. Fuerte-Esquivel, and V. M. Chavez-Ornelas, "Modeling of static VAR's compensators in fast decoupled load flow," *IEEE Trans. Power Syst.*, vol. 20, no. 1, pp. 512–514, Feb. 2005.

[14] J. V. Milanovic and Y. Zhang, "Modeling of FACTS devices for voltage sag mitigation studies in large power systems," *IEEE Trans. Power Del.*, vol. 25, no. 4, pp. 3044–3052, Oct. 2010.

[15] J. Zhu, K. Cheung, D. Hwang, and A. Sadjadpour, "Operation strategy for improving voltage profile and reducing system loss," *IEEE Trans. Power Del.*, vol. 25, no. 1, pp. 390–397, Jan. 2010.

[16] L. F. W. De Souza, E. H. Watanabe, and M. Aredes, "GTO controlled series capacitors: Multi-module and multi-pulse arrangements," *IEEE Trans. Power Del.*, vol. 15, no. 2, pp. 725–731, Apr. 2000.

[17] K. Li, J. Zhao, C. Zhang, and W. Lee, "Dynamic simulator for thyristor-controlled series capacitor," *IEEE Trans. Ind. Appl.*, vol. 46, no. 3, pp. 1096–1102, May/Jun. 2010.

[18] N. Kakimoto and A. Phongphanphanee, "Subsynchronous resonance damping control of thyristor-controlled series capacitor," *IEEE Trans. Power Del.*, vol. 18, no. 3, pp. 1051–1059, Jul. 2003.

[19] L. A. Pilotto, A. Bianco, W. F. Long, and A.-A. Edris, "Impact of TCSC control methodologies on subsynchronous oscillations," *IEEE Trans. Power Del.*, vol. 18, no. 1, pp. 243–252, Jan. 2003.

[20] A. Swetapadma and A. Yadav, "Improved fault location algorithm for multi-location faults, transforming faults and shunt faults in thyristor-controlled series capacitor compensated transmission line," *IET Gener. Transmiss. Distrib.*, vol. 9, no. 13, pp. 1597–1607, Oct. 2015.
[21] M. Farahani, "Damping of subsynchronous oscillations in power system using static synchronous series compensator," *IET Gener. Transmiss. Distrib.*, vol. 6, no. 6, pp. 539–544, Jun. 2012.
[22] A. C. Pradhan and P. W. Lehn, "Frequency-domain analysis of the static synchronous series compensator," *IEEE Trans. Power Del.*, vol. 21, no. 1, pp. 440–449, Jan. 2006.
[23] L. Wang and Q.-S. Vo, "Power flow control and stability improvement of connecting an offshore wind farm to a one-machine infinite-bus system using a static synchronous series compensator," *IEEE Trans. Sustain. Energy*, vol. 4, no. 2, pp. 358–369, Apr. 2013.
[24] M. Saradarzadeh, S. Farhangi, J.-L. Schanen, P.-O. Jeannin, and D. Frey, "Application of cascaded H-bridge distribution-static synchronous series compensator in electrical distribution system power flow control," *IET Power Electron.*, vol. 5, no. 9, pp. 1660–1675, Nov. 2012.
[25] F. A. Jowder, "Influence of mode of operation of the SSSC on the small disturbance and transient stability of a radial power system," *IEEE Trans. Power Syst.*, vol. 20, no. 2, pp. 935–942, May 2005.
[26] W. Qiao, G. K. Venayagamoorthy, and R. G. Harley, "Missing-sensor-fault-tolerant control for SSSC FACTS device with real-time implementation," *IEEE Trans. Power Del.*, vol. 24, no. 2, pp. 740–750, Apr. 2009.
[27] B. Chen, W. Fei, C. Tian, and J. Yuan, "Research on an improved hybrid unified power flow controller," *IEEE Trans. Ind. Appl.*, vol. 54, no. 6, pp. 5649–5660, Nov./Dec. 2018.
[28] F. Z. Peng, Y. Liu, S. Yang, S. Zhang, D. Gunasekaran, and U. Karki, "Transformer-less unified power-flow controller using the cascade multilevel inverter," *IEEE Trans. Power Electron.*, vol. 31, no. 8, pp. 5461–5472, Aug. 2016.
[29] L. Liu, P. Zhu, Y. Kang, and J. Chen, "Power-flow control performance analysis of a unified power-flow controller in a novel control scheme," *IEEE Trans. Power Del.*, vol. 22, no. 3, pp. 1613–1619, Jul. 2007.
[30] S. P. Singh, "Congestion mitigation using UPFC," *IET Gener. Transmiss. Distrib.*, vol. 10, no. 10, pp. 2433–2442, Jul. 2016.
[31] Z. Moravej, M. Pazoki, and M. Khederzadeh, "New pattern-recognition method for fault analysis in transmission line with UPFC," *IEEE Trans. Power Del.*, vol. 30, no. 3, pp. 1231–1242, Jun. 2015.
[32] M. A. Sayed and T. Takeshita, "Line loss minimization in isolated substations and multiple loop distribution systems using the UPFC," *IEEE Trans. Power Electron.*, vol. 29, no. 11, pp. 5813–5822, Nov. 2014.
[33] S. Golshannavaz, F. Aminifar, and D. Nazarpour, "Application of UPFC to enhancing oscillatory response of series-compensated wind farm integrations," *IEEE Trans. Smart Grid*, vol. 5, no. 4, pp. 1961–1968, Jul. 2014.
[34] Y. Zhang and X. Ruan, "AC–AC converter with controllable phase and amplitude," *IEEE Trans. Power Electron.*, vol. 29, no. 11, pp. 6235–6244, Nov. 2014.
[35] Y. Zhang and X. Ruan, "Three-phase ac–ac converter with controllable phase and amplitude," *IEEE Trans. Ind. Electron.*, vol. 62, no. 9, pp. 5689–5699, Sep. 2015.
[36] Y. Zhang and X. Ruan, "π model ac–ac converter with controllable phase and amplitude," *IEEE Trans. Ind. Electron.*, vol. 64, no. 8, pp. 6422–6431, Aug. 2017.
[37] Y. Zhang, H. Jin, and Y. Zhang, "Full-duty-cycle regulated three-level ac–ac converter with self-following flying capacitor," *IEEE Access*, vol. 6, no. 9, pp. 48428–48437, Aug. 2018.

Youjun Zhang was born in Huangshan, Anhui Province, China, in 1970. He received the B.S. degree in electrical engineering from Southwest Jiaotong University, Chengdu, China, in 1992, and the M.S. and Ph.D. degrees in electrical engineering from Nanjing University of Aeronautics and Astronautics, Nanjing, China, in 2002 and 2014, respectively.

In 2004, he joined the School of Mechanical and Electrical Engineering, Soochow University, Suzhou, China, where he became a Professor in 2018. He has been a Coresearcher with the Jiangsu Key Laboratory of Spectral Imaging & Intelligent Sense and Ministerial Key Laboratory of JGMT, Nanjing University of Science and Technology, Nanjing, since 2014 and 2016, respectively. His main research interests include ac/ac converters for power flow control, multilevel converters, and dc/ac converters.

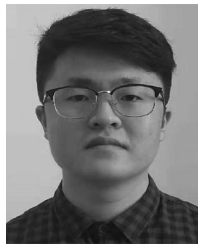

Guoqing Lu was born in Fuyang, Anhui Province, China, in 1995. He received the B.S. degree in mechanical design manufacturing and automation from Anhui University of Technology, Maanshan, China, in 2017. He is currently working toward the M.S. degree in control engineering at Soochow University, Suzhou, China.

His main research interests include power electronics, especially focusing on ac/ac converters for power flow control.

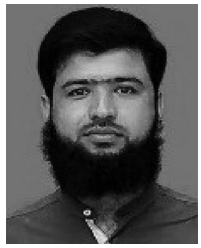

Wajid Ali Khan was born in Swat, Khyber Pakhtunkhwa, Pakistan, in 1993. He received the B.S. degree in electrical engineering from the University of Engineering and Technology, Peshawar, Pakistan, in 2016. He is currently working toward the M.S. degree in control engineering at Soochow University, Suzhou, China.

His research interests include power electronics, especially multilevel converters and ac/ac converters.

Yuzhen Zhang was born in Huangshan, Anhui Province, China, in 1973. She received the B.S. degree in industrial automation instrument from Anhui University of Technology, Maanshan, China, in 1996, the M.S. degree in control science and engineering from Southeast University, Nanjing, China, in 2003, and the Ph.D. degree in control science and engineering from the Nanjing University of Science and Technology, Nanjing, China, in 2013.

In 2003, she joined the School of Automation, Nanjing University of Science and Technology, Nanjing, China. In 2010, she joined the Jiangsu Key Laboratory of Spectral Imaging & Intelligent Sense, Nanjing University of Science and Technology, where she became an Associate Professor in 2014.

Qixin Zhu was born in Dingyuan, Anhui Province, China, in 1971. He received the B.S. and M.S. degrees in industrial automation from Xi'an Polytechnic University, Xi'an, China, in 1994 and 1997, respectively, and the Ph.D. degree in control theory and control engineering from the Nanjing University of Aeronautics and Astronautics, Nanjing, China, in 2003.

He was with Nantong University, Nantong, China, from April 1997 to July 2004, with ASM Assembly Automation Ltd., Hong Kong, China, from July 2004 to August 2006, and with East China Jiaotong University, Nanchang, China, from August 2006 to February 2013. He is currently a Professor with the School of Mechanical Engineering, Suzhou University of Science and Technology, Suzhou, China.